The *Caenorhabditis elegans* Lifespan Machine

Nicholas Stroustrup[1], Bryne E Ulmschneider[1], Zachary M Nash[1], Isaac F López-Moyado[1], Javier Apfeld[1,2] & Walter Fontana[1,2]

The measurement of lifespan pervades aging research. Because lifespan results from complex interactions between genetic, environmental and stochastic factors, it varies widely even among isogenic individuals. The actions of molecular mechanisms on lifespan are therefore visible only through their statistical effects on populations. Indeed, survival assays in *Caenorhabditis elegans* have provided critical insights into evolutionarily conserved determinants of aging. To enable the rapid acquisition of survival curves at an arbitrary statistical resolution, we developed a scalable imaging and analysis platform to observe nematodes over multiple weeks across square meters of agar surface at 8-μm resolution. The automated method generates a permanent visual record of individual deaths from which survival curves are constructed and validated, producing data consistent with results from the manual method of survival curve acquisition for several mutants in both standard and stressful environments. Our approach permits rapid, detailed reverse-genetic and chemical screens for effects on survival and enables quantitative investigations into the statistical structure of aging.

Aging organisms exhibit functional declines at many levels of biological organization. These declines ultimately kill the organism and thus determine its lifespan. Because lifespans vary remarkably[1] even within isogenic populations, useful information about aging mechanisms can be obtained by characterizing the response of lifespan distributions to genetic, chemical and physical interventions.

C. elegans individuals live as self-fertile adults for a few weeks, producing large numbers of isogenic offspring. Early investigations revealed single point mutations in insulin/IGF-1 pathway components that were capable of doubling the average lifespan[2–5]. These findings were subsequently generalized to other organisms, including fruit flies and mice[5], establishing *C. elegans* as a metazoan model for studying the genetics of aging. The acquisition of survival curves in *C. elegans* thus became an essential part of aging research. In routine practice, survival curves of animals cultured on solid agar in a Petri dish, and fed by a bacterial lawn of *Escherichia coli*, are acquired manually through daily observation with a low-power dissecting microscope[6,7]. Death is recognized by the failure of an individual to move in reaction to prodding with a wire, a methodology that requires labor-intensive, repetitive

and subjective observation. Such a protocol provides strong incentives to keep population sizes small, observations infrequent and the number of replicates limited, thus curtailing the reproducibility and scope of data collected.

We present a scalable method for producing survival curves at any desired statistical resolution, allowing 'hands-free', lifelong and accurate observation of large nematode populations. Our method combines groups of flatbed scanners so that they function as a single spatially extended microscope. Alone or in groups, these scanners produce time-lapse videos under highly controlled environmental conditions. We couple this imaging approach with an image-analysis pipeline that automatically identifies death times. By creating an auditable trail of images, the system allows rapid validation and refinement of processed data and therefore supports a statistically rigorous analysis of aging and stress resistance.

In several cases, notably in worms and flies, focused efforts have been made to acquire high-resolution survival data[8–15]. Our method standardizes such observations for nematodes, enabling the accumulation of quantitative demographic data that tightly link aging, genotype and environment. We refer to the integrated combination of scanner hardware and image-processing software as the Lifespan Machine (LM; http://www.lifespanmachine.org/).

RESULTS
A distributed microscope for large worm populations
Lifespan data are acquired over many scales, from aging studies spanning multiple months to stress-resistance assays lasting less than a day[16], and they can involve targeted characterizations of only a few strains[12] or screening projects of thousands of gene knockdowns[2,3,5]. Throughput is important for screening projects, and targeted studies benefit from the statistical power that large populations provide. To suit all these purposes, our platform combines flatbed scanners in a scalable fashion to monitor arbitrarily large populations over a wide range of timescales.

Our approach replaces human observation with an automated system that acquires and processes time-lapse images to identify the timing of death, which is defined as the persistent cessation of spontaneous movement. Our current reference implementation can monitor 30,000 animals across 800 plates simultaneously, imaging 1.57 m^2 of agar surface at a resolution of 8 μm (**Supplementary Notes 1–4**). This capacity is used to run many

[1]Department of Systems Biology, Harvard Medical School, Boston, Massachusetts, USA. [2]These authors contributed equally to this work. Correspondence should be addressed to N.S. (nstroustrup@post.harvard.edu), J.A. (javier_apfeld@hms.harvard.edu) or W.F. (walter@hms.harvard.edu).
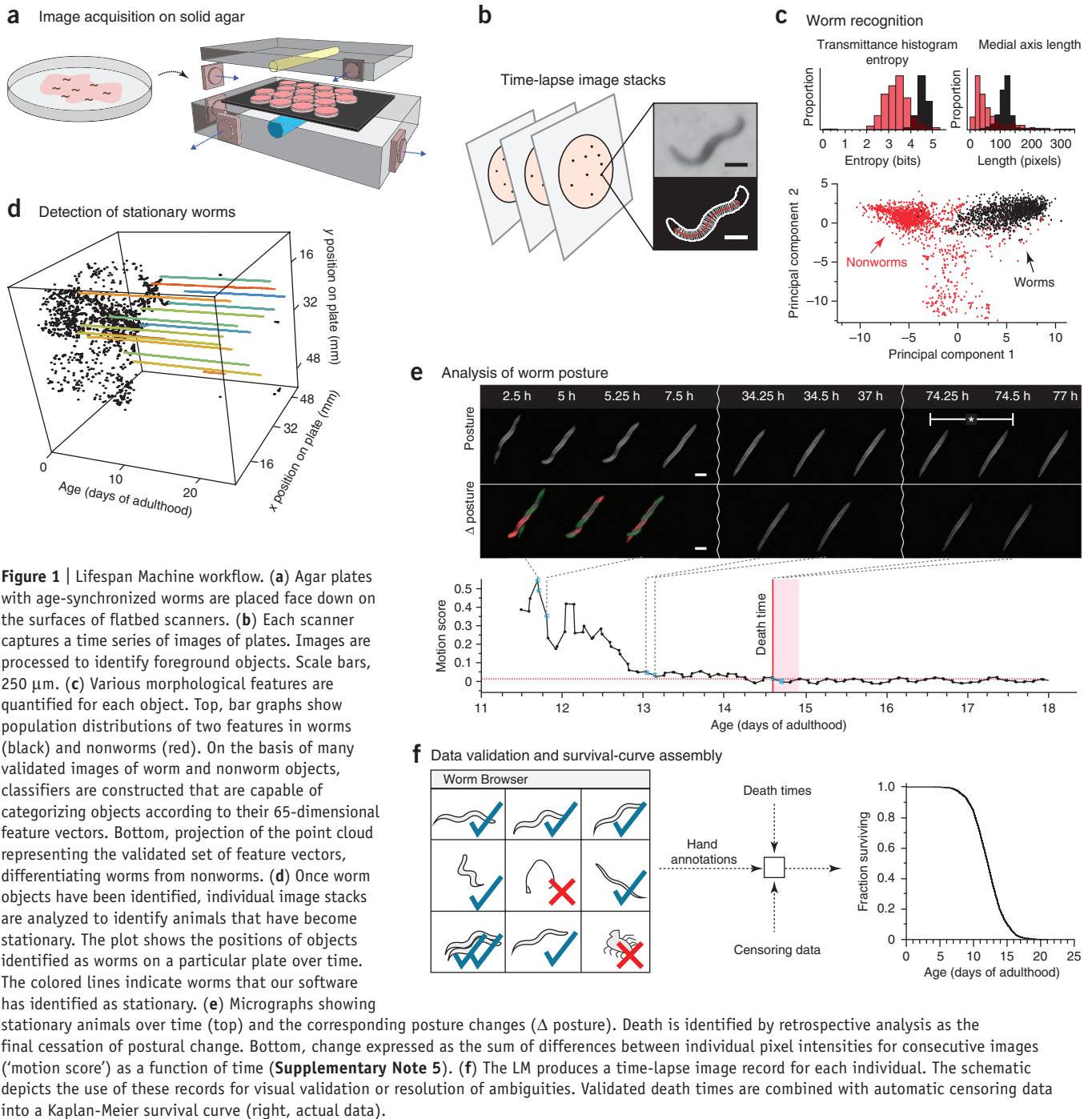
a Image acquisition on solid agar

b Time-lapse image stacks

c Worm recognition

Transmittance histogram entropy

Medial axis length

d Detection of stationary worms

e Analysis of worm posture

| 2.5 h | 5 h | 5.25 h | 7.5 h | 34.25 h | 34.5 h | 37 h | 74.25 h | 74.5 h | 77 h |

Posture

Δ posture

f Data validation and survival-curve assembly

Worm Browser

Death times

Hand annotations

Censoring data

Figure 1 | Lifespan Machine workflow. (**a**) Agar plates with age-synchronized worms are placed face down on the surfaces of flatbed scanners. (**b**) Each scanner captures a time series of images of plates. Images are processed to identify foreground objects. Scale bars, 250 μm. (**c**) Various morphological features are quantified for each object. Top, bar graphs show population distributions of two features in worms (black) and nonworms (red). On the basis of many validated images of worm and nonworm objects, classifiers are constructed that are capable of categorizing objects according to their 65-dimensional feature vectors. Bottom, projection of the point cloud representing the validated set of feature vectors, differentiating worms from nonworms. (**d**) Once worm objects have been identified, individual image stacks are analyzed to identify animals that have become stationary. The plot shows the positions of objects identified as worms on a particular plate over time. The colored lines indicate worms that our software has identified as stationary. (**e**) Micrographs showing stationary animals over time (top) and the corresponding posture changes (Δ posture). Death is identified by retrospective analysis as the final cessation of postural change. Bottom, change expressed as the sum of differences between individual pixel intensities for consecutive images ('motion score') as a function of time (**Supplementary Note 5**). (**f**) The LM produces a time-lapse image record for each individual. The schematic depicts the use of these records for visual validation or resolution of ambiguities. Validated death times are combined with automatic censoring data into a Kaplan-Meier survival curve (right, actual data).

independent, single-scanner experiments in parallel with larger investigations involving ten scanners or more.

Young worms move quickly relative to the observation frequency attainable with scanners, which precludes their tracking. However, as animals slow down with age, their motion can be quantified longitudinally, especially when it is limited to changes in posture at a fixed location.

Each scanner monitors 16 Petri dishes (plates) sealed face down to a glass sheet by a rubber mat, with each plate containing a population of about 35 animals (Online Methods). A fluorescent lamp inside the scanner lid sends light through the plates, agar, bacteria and worms and is captured by a sensor chip moving

underneath the glass surface in synchrony with the light source (**Fig. 1a** and **Supplementary Notes 1** and **3**). A scanner thus acts as 16 camera-equipped dissecting microscopes but costs significantly less and has dimensions suited for dense shelving inside temperature-controlled incubators.

In traditional protocols for monitoring large populations of nematodes over long periods of time, plates are moved in and out of an incubator[6,7], which exposes them to spatially and temporally heterogeneous conditions. Our apparatus maintains each plate at a fixed position in a controlled environment for the duration of each experiment. This is important for accuracy, given the exquisite temperature sensitivity of the *C. elegans* lifespan[17]

Figure 2 | Automated wild-type survival data. (**a**) Per-plate survival curves from 484 wild-type animals distributed over 13 plates located on a single scanner ("Machine," top) and 513 wild-type animals distributed over 10 plates observed using the manual method ("By hand," bottom). (**b**) A population of 3,578 wild-type animals on ten scanners was aggregated into a single curve and compared to the aggregated manually scored curves from **a**. (**c**) Scanner-specific microenvironments affect lifespan (top); this variation can be corrected (bottom) using estimations from a categorical accelerated failure time model. (**d**) Hazard rates were estimated from lifespan data. The blue (Weibull) and red (Gompertz) lines represent maximum-likelihood estimation (MLE) fits of the parametric model using data up to median survival. (**e**) Image records of populations on two scanners were selected for validation to determine death times by eye and by the automated method. (**f**) Cumulative LM error (the death-time differences between automation and visual inspection) for both scanners. Visual and automatic lifespans are highly correlated ($R^2 = 0.96$, inset).

(**Supplementary Note 1**). We curbed temperature excursions with two systems of fans: one system to cool each scanner and the other to circulate air evenly throughout the enclosing incubator (**Supplementary Note 3**). Temperature fluctuations on a typical scanner surface were thus reduced from several degrees to less than 0.5 °C, and temperature differences between scanners were limited to about 1 °C (**Supplementary Note 1**).

To improve image quality, we repositioned a single fixed lens in the scanner's optical path, shifting the focal plane a few millimeters above the scanner glass to match the position of the agar surface inside the plates. To ensure that the agar surface is consistent across experiments, we developed a robust method for the controlled drying of agar plates (Online Methods).

Automated identification of death times

Following an optimized scanning schedule (Online Methods), the LM captures 24 images of each plate per day. The image-processing pipeline identifies worm objects (**Supplementary Note 2**) and their position in every frame (**Fig. 1b,c**). Once stationary (**Fig. 1d**), individual animals continue to change posture for a time, often moving their head or tail (**Fig. 1e**, **Supplementary Videos 1–5** and **Supplementary Note 5**): a behavior reminiscent of the 'class C' animals described in studies of age-dependent locomotory decline[18]. Our software determines the final cessation of spontaneous postural movement through retrospective image analysis (Online Methods, **Supplementary Note 5** and **Supplementary Video 6**). Posture analysis of stationary animals is crucial for avoiding underestimation of lifespan. We observed wild-type animals spending on average 1.2 d of their life in this state (**Fig. 1e**), whereas certain mutants, such as *age-1*(*hx546*), persisted in this state more than twice as long (**Supplementary Note 6**), a result consistent with previous reports[19].

We found that most animals exhibited a stereotypical morphological change at or near the time of their final posture change (**Supplementary Note 7**). Individuals first shrank by at least 10% and afterward expanded by more than that amount. We never observed a change in posture after this expansion. The correlation between the cessation of postural motion and this morphological change suggests a physiological transition, perhaps one corresponding to the animal's death, corroborating our death criterion.

A crucial component of our platform is a software package that allows rapid validation of death times through visual inspection (**Supplementary Note 4**). This quality-control step (**Fig. 1f**,
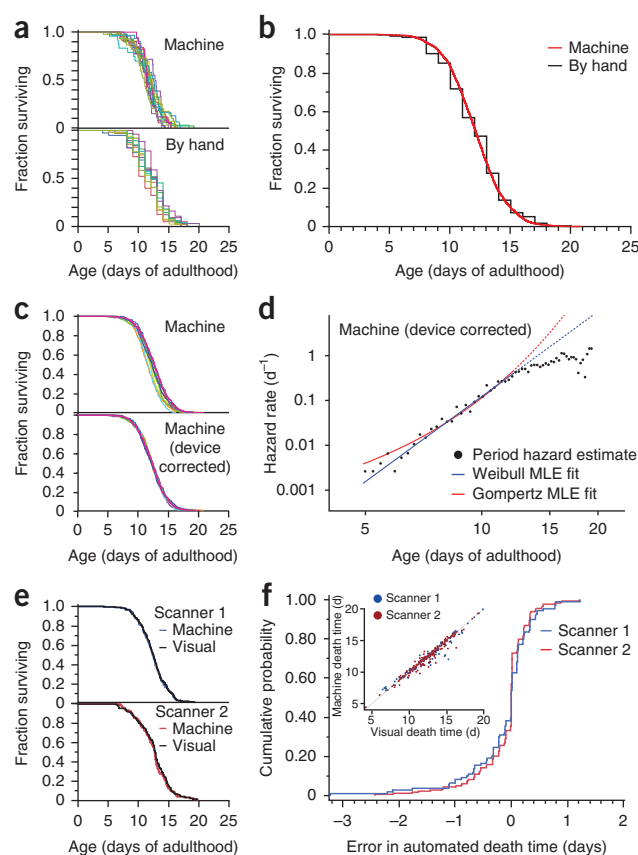
Supplementary Video 6 and Online Methods) allows a user to determine whether plates have been compromised (for example, by desiccation or fungal contamination) and need to be excluded from analysis. In particular, it permits identification of aggregates containing multiple worms (**Supplementary Note 8**) and the censoring of incorrectly classified objects (such as features of the agar lawn) and non–aging-related deaths (such as body rupture), thus enabling a visual validation of machine operation.

The LM produces accurate and precise survival curves

To evaluate whether the LM produces results consistent with those of a human observer, we placed roughly 8,000 age-synchronous wild-type animals into a single liquid suspension and distributed aliquots of approximately 35 individuals per plate across 170 agar plates seeded with *E. coli* OP50 (Online Methods). Of these plates, 160 were distributed across ten scanners situated in an incubator at 25 °C. The remaining ten plates were placed in a separate incubator and monitored daily by hand using a dissecting microscope.

Because we drew all animals from the same pool, any significant difference between survival curves of individual plates must be attributed to either measurement error or environmental variation, such as differences in plate temperature. We compared death times grouped by plate on a single scanner with those acquired by the manual procedure (**Fig. 2a**). In both methods, plate means varied within essentially the same range, between 10.7 and 13.1 d (individual death times are provided in the **Supplementary Data**, and summary statistics of all data shown are reported in **Supplementary Table 1**). No significant effect was observed between plates collected by the manual method (log-rank test
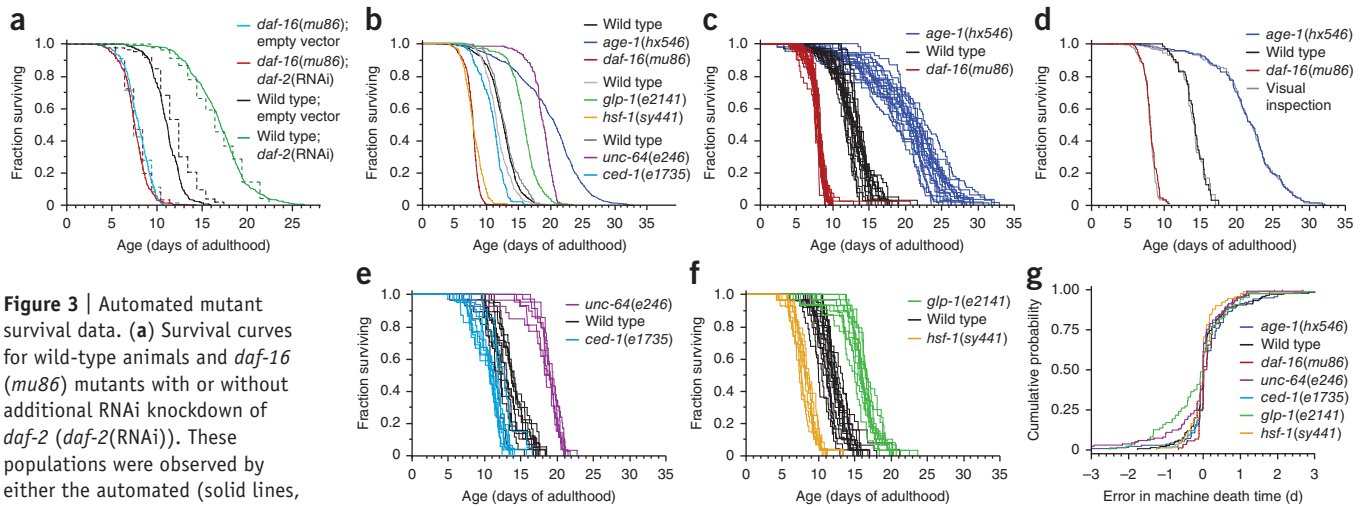
Figure 3 | Automated mutant survival data. (**a**) Survival curves for wild-type animals and *daf-16* (*mu86*) mutants with or without additional RNAi knockdown of *daf-2* (*daf-2*(RNAi)). These populations were observed by either the automated (solid lines, 2,015 animals) or manual (dashed lines, 541 animals) method. (**b**–**f**) Survival curves for six mutant populations monitored by the LM. Their lifespan data are shown both aggregated (**b**) and, in subsequent panels, grouped by plate. Each panel pair in **c**,**e**,**f** refers to a separate scanner also running a wild-type population as reference. The population sizes were *daf-16*(*mu86*), 654; wild type, 594; *age-1*(*hx546*), 1,109 (**c**); *ced-1*(*e1735*), 255; wild type, 314; *unc-64*(*e246*), 193 (**e**); and *hsf-1*(*sy441*), 234; wild type, 472; *glp-1*(*e2141*), 335 (**f**). (**d**) Comparison between survival curves determined from visually and automatically scored death times, as in **Figure 2e**. Comparisons for all other mutants are shown in **Supplementary Note 13**. (**g**) Cumulative LM error, as in **Figure 2f**, for each mutant population.

for homogeneity $P = 0.059$). A small, significant difference was observed between plates collected by the automated method (log-rank $P = 0.002$), reflecting either inaccuracies in the estimation of death times or a slightly increased environmental variability among plates. In two independent replicates, the aggregated survival curves determined by the LM differed in mean lifespan by 2.5 h, or 0.2% (log-rank $P = 0.01$, **Fig. 2b**), and 11.7 h, or 3.2% (log-rank $P < 0.0001$), from those of the aggregated cohorts assayed using the conventional method.

For experiments that require comparison between populations much larger than 300 individuals, animals must be distributed across multiple scanners. With the statistical power (**Supplementary Note 9**) afforded by each scanner, even slight environmental differences between scanners translated into statistically significant differences between survival curves (**Fig. 2c**). Scanner surface temperature correlated well with mean lifespan ($R^2 = 0.75$; $P = 0.023$; **Supplementary Note 1**). Because devices produced a small effect on lifespan, we applied an accelerated-failure-time regression model with scanner identity as a categorical covariate to generate 'device-corrected' lifespans (**Fig. 2c** and **Supplementary Note 10**). This procedure is useful for assessing whether data pooling is justified and for standardizing data against a desired baseline curve: for example, aligning large experiments to a single scanner.

The LM provides data in a quantity and quality appropriate for estimating[20] the time-dependent hazard (mortality) rate, which refers to the instantaneous probability that an individual of age t dies in the next instant (**Supplementary Note 11**). We observed a rapid increase and subsequent deceleration in mortality with time, as noted previously[10–12,14]. For the first 50% of deaths, mortality appears better fit by a power of time t (Weibull hazard, $\alpha/\beta\,(t/\beta)^{\alpha-1}$) than by an exponential in time (Gompertz hazard, $ae^{t/b}$)(**Fig. 2d** and **Supplementary Note 11**). However, for values of the Gompertz parameter a much smaller than 1, Gompertz and Weibull distributions behave very similarly for all but the

lowest quantiles of survival, making disambiguation difficult. An analysis of the full hazard data, accounting for the deceleration phase, may require frailty models to incorporate phenotypic diversity potentially present even in isogenic populations[21,22]. The observed hazard deceleration was not the result of environmental heterogeneity between scanners, as it persisted after device correction (data not shown).

The close agreement between automated and manual survival curves was surprising, as scanners expose animals to conditions that differ from the manual method: for example, oscillating lights[23] and temperature oscillations (**Supplementary Note 1**). The difference in lifespan between animals exposed and those unexposed to the scanner environment, but scored by hand, was so small that it could be explained by limitations in our ability to maintain the same temperature in both environments (**Supplementary Note 12**). Likewise, small differences between curves from LM replicates, and between LM curves and those from manual controls, could be explained by slight overall temperature differences due to variation in the physical setup. Notably, the LM and the manual procedure adopt different operational definitions of death: cessation of spontaneous versus of stimulated movement, respectively. We therefore sought a validation process other than comparison to the manual method by developing software (the Worm Browser) to assist in the visual inspection of the image record generated by the LM (**Supplementary Note 4** and **Supplementary Video 6**). Two survival curves constructed from 294 user-annotated death times based on images from two scanners were each statistically indistinguishable from curves produced by automated annotation (log-rank $P > 0.5$; **Fig. 2e**,**f**).

The LM reproduces known lifespans of genetic perturbations

To test whether the LM could be used to characterize the effects of mutations and RNAi on lifespan, we divided wild-type animals and *daf-16*(*mu86*) mutants[3] between plates seeded with either an *E. coli* HT115(DE3) strain containing an RNAi construct targeting

Figure 4 | Automated stress-resistance assays. (**a**,**b**) LM-acquired survival curves for age-synchronous populations of 1,873 *age-1*(*hx546*) mutants, 2,106 *daf-16*(*mu86*) mutants and 1,726 wild-type animals transferred to 35 °C on their second day of adulthood. Populations of individual plates (**a**) and aggregates (**b**) for all animals of each genotype are shown. (**c**) LM operation validated as in **Figure 2e** (log-rank *P* > 0.5 in all cases). (**d**,**e**) LM-acquired survival curves for populations of *age-1*(*hx546*), wild-type and *daf-16*(*mu86*) animals that were transferred onto agar treated with 3 mM *t*-BuOOH (2,135 animals) (**d**) or 6 mM *t*-BuOOH (1,808 animals total) (**e**) at 25 °C. (**f**) LM-acquired survival curves obtained from populations of 1,306 *C. elegans* (N2 Bristol isolate), 255 *C. elegans* (Hawaiian isolate), 285 *C. briggsae*, 224 *C. species 11* and 295 *C. brenneri* nematodes raised on live *E. coli* OP50 at 20 °C and transferred to 34.5 °C on the second day of adulthood.
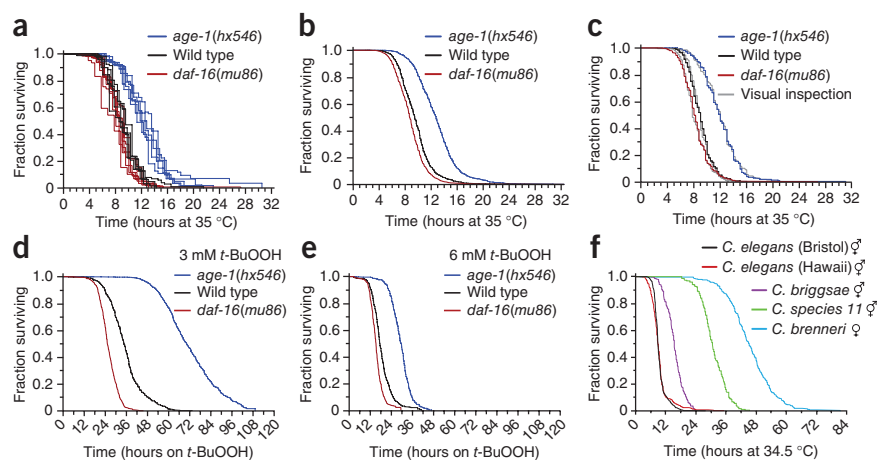
the insulin/IGF receptor *daf-2* (refs. 3,24) or an empty vector. As expected, *daf-16* mutants lived less long than wild-type animals[25], and knockdown of *daf-2* by RNAi extended the lifespan of wild-type animals but not *daf-16* mutants[24] (**Fig. 3a**). We found no significant difference between manual and automated survival curves for all conditions (log-rank *P* > 0.3) except wild-type animals feeding on control bacteria (log-rank *P* < 0.0001), which appeared to live 21 h longer in the manual assay. A subsequent replicate showed a much smaller effect (**Supplementary Note 12**). These experiments were performed at 25 °C; we observed corresponding effects at 20 °C (**Supplementary Note 13**).

Consistent with previous reports[2,5,25–27], mutations in the phosphoinositide 3-kinase *age-1*, the syntaxin homolog *unc-64* and the Notch receptor *glp-1* resulted in lifespan extension, whereas mutations in *daf-16*, the heat-shock factor *hsf-1* and the CD91 homolog *ced-1* shortened lifespan. Our automated technique correctly identified known genetic determinants of *C. elegans* lifespan (**Fig. 3b**–**g**).

Through visual image inspection (**Fig. 3d,g**), we validated the LM-acquired survival curves of mutants. We note that the machine performed well on the movement-defective mutants *unc-64*(*e246*), *unc-4*(*e120*), *unc-50*(*e306*) and *unc-119*(*ed3*) (**Supplementary Note 13**) even though the image-analysis parameters were optimized for detecting wild-type movement. The LM performed equally well for *glp-1*(*e2141*) and wild type despite mutant animals being thinner from the absence of a germ line.

The LM enables high-resolution stress-resistance assays

Survival assays are widely used to evaluate the ability of individuals to withstand exogenous stresses. Exposure to high temperature (35 °C) or toxins dramatically shortens the lifespan of *C. elegans*. Mean survival can range from several hours to a few days[16,28], making data collection at high frequency challenging for the manual approach. We evaluated the performance of the LM in two stress-resistance scenarios: exposure to high temperature[16] and to the oxidant *tert*-butyl hydroperoxide (*t*-BuOOH)[28]. The LM required no modifications beyond adjustments to a subset of parameters used by our image-analysis software to quantify worm movement and identify worm death times (Online Methods).

Age-synchronous wild-type animals and *age-1*(*hx546*) and *daf-16*(*mu86*) mutants were grown under standard conditions at 25 °C and shifted on the second day of adulthood to one of four conditions: oxidant-free agar plates at 25 °C or 35 °C or agar plates with 3 mM or 6 mM *t*-BuOOH at 25 °C. Although no wild-type animals died during the first 2 d on control plates at 25 °C, their lifespans were shortened dramatically at 35 °C. In agreement with previous reports[16], *age-1*(*hx546*) mutants lived longer than wild type at 35 °C, and *daf-16*(*mu86*) mutants showed a small but statistically significant reduction in survival (*P* < 0.0001) (**Fig. 4a,b**). The results obtained by visual and automated image analyses were highly correlated (**Fig. 4c** and **Supplementary Note 13**). We observed a similar, concentration-dependent effect of *t*-BuOOH on lifespan that is consistent with previous studies[28] (**Fig. 4d,e**). The LM is therefore well suited for assaying the effects of chemicals on survival in *C. elegans*.

Despite a separation of 100 million years or more[29], the *Caenorhabditis* species *elegans*, *briggsae*, *brenneri* and *species 11* are sufficiently similar in appearance for the LM to function correctly with no additional calibration at 35 °C (**Fig. 4f**). We confirmed previous reports[30] that *Caenorhabditis briggsae* and *Caenorhabditis brenneri* are more thermotolerant than *C. elegans*, and we found this higher thermotolerance to be the case for *Caenorhabditis species 11* as well. The thermotolerance profiles of these species correlate with the temperatures of their natural habitats[29], with tropical species being more thermotolerant than temperate ones.

DISCUSSION

By using standard nematode culture conditions, our method meaningfully extends the existing experimental literature and can be checked against it. Our approach has several limitations (**Supplementary Note 14**), the most significant one being the inaccessibility of animals during automated observation, as plates and scanners must remain unperturbed. This inability to handle animals can be somewhat mitigated by delaying automated observation until after the necessary handling is complete. If interventions are performed primarily during the reproductive period, the vast majority of death events can still be acquired automatically.

The modular design of the LM gives researchers the flexibility to expand an installation by simply adding scanners (**Supplementary Notes 15** and **16**). A single scanner is sufficient to compare the lifespan of a mutant population against a wild-type control, detecting 10% differences in survival with 99% confidence and 99% power. Facilities of ten or more scanners can provide sufficient throughput to systematically characterize the effects of many genes and environmental conditions on survival. At an even larger scale, we can pair scope with depth by evaluating populations that are large enough that hazard-rate features can be resolved and quantitatively compared, thus linking interventions at the molecular level with their statistical footprint at the organismic level.

METHODS
Methods and any associated references are available in the online version of the paper.

Note: Supplementary information is available in the online version of the paper.

AUTHOR CONTRIBUTIONS
N.S. designed and implemented hardware and software. N.S. and B.E.U. constructed and calibrated equipment. N.S. and J.A. conceived and designed experiments. N.S., B.E.U., J.A., Z.M.N. and I.F.L.-M. performed experiments. N.S. designed analytic tools. N.S., J.A. and W.F. provided guidance, analyzed data, interpreted results and wrote the manuscript. J.A and W.F. are co-last authors.

1. Kirkwood, T.B. *et al.* What accounts for the wide variation in life span of genetically identical organisms reared in a constant environment? *Mech. Ageing Dev.* **126**, 439–443 (2005).
2. Friedman, D.B. & Johnson, T.E. A mutation in the *age-1* gene in *Caenorhabditis elegans* lengthens life and reduces hermaphrodite fertility. *Genetics* **118**, 75–86 (1988).
3. Kenyon, C., Chang, J., Gensch, E., Rudner, A. & Tabtiang, R. A *C. elegans* mutant that lives twice as long as wild type. *Nature* **366**, 461–464 (1993).
4. Kimura, K.D., Tissenbaum, H.A., Liu, Y. & Ruvkun, G. *daf-2*, an insulin receptor-like gene that regulates longevity and diapause in *Caenorhabditis elegans*. *Science* **277**, 942–946 (1997).
5. Kenyon, C.J. The genetics of ageing. *Nature* **464**, 504–512 (2010).
6. Sutphin, G.L. & Kaeberlein, M. Measuring *Caenorhabditis elegans* life span on solid media. *J. Vis. Exp.* **12**, pii: 1152 (2009).
7. Wilkinson, D.S., Taylor, R.C. & Dillin, A. Analysis of aging in *Caenorhabditis elegans*. *Methods Cell Biol.* **107**, 353–381 (2012).
8. Curtsinger, J.W., Fukui, H.H., Townsend, D.R. & Vaupel, J.W. Demography of genotypes: failure of the limited life-span paradigm in *Drosophila melanogaster*. *Science* **258**, 461–463 (1992).
9. Carey, J.R., Liedo, P. & Vaupel, J.W. Mortality dynamics of density in the Mediterranean fruit fly. *Exp. Gerontol.* **30**, 605–629 (1995).
10. Vaupel, J.W. *et al.* Biodemographic trajectories of longevity. *Science* **280**, 855–860 (1998).
11. Vanfleteren, J.R., De Vreese, A. & Braeckman, B.P. Two-parameter logistic and Weibull equations provide better fits to survival data from isogenic populations of *Caenorhabditis elegans* in axenic culture than does the Gompertz model. *J. Gerontol. A Biol. Sci. Med. Sci.* **53**, B393–B408 (1998).
12. Johnson, T.E., Wu, D., Tedesco, P., Dames, S. & Vaupel, J.W. Age-specific demographic profiles of longevity mutants in *Caenorhabditis elegans* show segmental effects. *J. Gerontol. A Biol. Sci. Med. Sci.* **56**, B331–B339 (2001).
13. Mair, W., Goymer, P., Pletcher, S.D. & Partridge, L. Demography of dietary restriction and death in *Drosophila*. *Science* **301**, 1731–1733 (2003).
14. Baeriswyl, S. *et al.* Modulation of aging profiles in isogenic populations of *Caenorhabditis elegans* by bacteria causing different extrinsic mortality rates. *Biogerontology* **11**, 53–65 (2010).
15. Wu, D., Rea, S.L., Cypser, J.R. & Johnson, T.E. Mortality shifts in *Caenorhabditis elegans*: remembrance of conditions past. *Aging Cell* **8**, 666–675 (2009).
16. Lithgow, G.J., White, T.M., Melov, S. & Johnson, T.E. Thermotolerance and extended life-span conferred by single-gene mutations and induced by thermal stress. *Proc. Natl. Acad. Sci. USA* **92**, 7540–7544 (1995).
17. Klass, M.R. Aging in the nematode *Caenorhabditis elegans*: major biological and environmental factors influencing life span. *Mech. Ageing Dev.* **6**, 413–429 (1977).
18. Herndon, L.A. *et al.* Stochastic and genetic factors influence tissue-specific decline in ageing *C. elegans*. *Nature* **419**, 808–814 (2002).
19. Huang, C., Xiong, C. & Kornfeld, K. Measurements of age-related changes of physiological processes that predict lifespan of *Caenorhabditis elegans*. *Proc. Natl. Acad. Sci. USA* **101**, 8084–8089 (2004).
20. Müller, H.G. & Wang, J.L. Hazard rate estimation under random censoring with varying kernels and bandwidths. *Biometrics* **50**, 61–76 (1994).
21. Vaupel, J.W., Manton, K.G. & Stallard, E. The impact of heterogeneity in individual frailty on the dynamics of mortality. *Demography* **16**, 439–454 (1979).
22. Weitz, J.S. & Fraser, H.B. Explaining mortality rate plateaus. *Proc. Natl. Acad. Sci. USA* **98**, 15383–15386 (2001).
23. Mathew, M.D., Mathew, N.D. & Ebert, P.R. WormScan: a technique for high-throughput phenotypic analysis of *Caenorhabditis elegans*. *PLoS ONE* **7**, e33483 (2012).
24. Dillin, A., Crawford, D.K. & Kenyon, C. Timing requirements for insulin/IGF-1 signaling in *C. elegans*. *Science* **298**, 830–834 (2002).
25. Larsen, P.L., Albert, P.S. & Riddle, D.L. Genes that regulate both development and longevity in *Caenorhabditis elegans*. *Genetics* **139**, 1567–1583 (1995).
26. Ailion, M., Inoue, T., Weaver, C.I., Holdcraft, R.W. & Thomas, J.H. Neurosecretory control of aging in *Caenorhabditis elegans*. *Proc. Natl. Acad. Sci. USA* **96**, 7394–7397 (1999).
27. Haskins, K.A., Russell, J.F., Gaddis, N., Dressman, H.K. & Aballay, A. Unfolded protein response genes regulated by CED-1 are required for *Caenorhabditis elegans* innate immunity. *Dev. Cell* **15**, 87–97 (2008).
28. Tullet, J.M. *et al.* Direct inhibition of the longevity-promoting factor SKN-1 by insulin-like signaling in *C. elegans*. *Cell* **132**, 1025–1038 (2008).
29. Kiontke, K.C. *et al.* A phylogeny and molecular barcodes for *Caenorhabditis*, with numerous new species from rotting fruits. *BMC Evol. Biol.* **11**, 339 (2011).
30. Amrit, F.R., Boehnisch, C.M. & May, R.C. Phenotypic covariance of longevity, immunity and stress resistance in the *Caenorhabditis* nematodes. *PLoS ONE* **5**, e9978 (2010).

ONLINE METHODS

***C. elegans* culture.** The following nematode strains were used: CB246 [*unc-64(e246)III*]; CB3203 [*ced-1(e1735)I*]; CF1037 [*daf-16 (mu86)I*]; HT1593 [*unc-119(ed3)III*]; N2 [wild type (Bristol)]; QZ112 [*hsf-1(sy441)I*]; QZ121 [*glp-1(e2141)III*]; TJ1052 [*age-1 (hx546)II*]; TJ1060 [*spe-9(hc88)I; fer-15(b26)II*]; and TJ1062 [*spe-9 (hc88)I; fer-15(b26) age-1(hx542)II*]. Worms were cultured under standard conditions[31] on 6-cm-diameter Petri dishes containing 12 ml of NGM agar (referred as 'standard plates'). For survival assays, worms were housed on 'assay plates': shallower, 5-cm-diameter plates (VWR 351006) containing 8 ml of NGM agar[31], in which $CaCl_2$ was omitted to prevent formation of an insoluble precipitate that reduces image quality; 22.5 µg/ml nystatin (Sigma N3503) to prevent fungal growth; and 10 µg/ml 5-fluoro-2-deoxyuridine (FUDR, Sigma) to eliminate live progeny.

Worms were grown at either 20 °C or 25 °C as noted and fed *E. coli* OP50, except in RNAi experiments, in which they were fed *E. coli* HT115 (DE3) bacterial strains. *hsf-1* animals failed to develop at 25 °C and were therefore cultured at 20 °C and transferred to 25 °C at the L4 molt, along with their wild-type control. *glp-1* animals were transferred as eggs from 20 °C to 25 °C, along with their wild-type control. The *glp-1* and *hsf-1* wild-type controls did not differ and are aggregated in **Figure 3b** and are not differentiated in **Figure 3f**.

We monitored the condition of all plates in every experiment by examining plate images and videos. Plates that exhibited fungal growth, contamination, desiccation, fogging or appeared otherwise compromised were excluded from analysis. On average 10% of plates were excluded in this way, primarily as the result of fogging or desiccation. The bacterial lawn remained present on the plate at the conclusion of each experiment and provided sufficient food for all animals on the plate. Seeding plates with more bacteria than what we normally used did not affect lifespan (data not shown).

We aimed to place roughly 35 animals on each plate under automated observation, thereby ensuring that sufficient bacteria were present to feed nematodes throughout each experiment, which we confirmed by visual inspection of bacterial lawns. Population sizes are not constrained by any step of image processing. When animals are deposited onto plates as a liquid suspension, a natural variation exists in the number of animals transferred per plate. For the wild-type population shown in **Figure 2b**, we found no correlation between population size and the mean lifespan of animals on each plate ($P = 0.67$). We also found no correlation between the population size and the frequency of multiworm clusters (**Supplementary Note 8**) observed on each plate ($P = 0.82$), which suggests that higher population densities are feasible, at least for wild-type animals.

Age synchronization. For survival assays, age-synchronous cohorts were prepared by hypochlorite treatment[7]. Eggs were washed in M9 buffer[31] 4–6 times and immediately placed on standard plates containing *E. coli*. Late-L4 larvae were transferred onto standard plates containing 10 µg/ml FUDR (established by visual inspection of vulval development). On the second day of adulthood, worms were transferred onto assay plates. Prior to being plated, we subjected wild-type eggs used in **Figure 2** to an additional synchronization step by arresting their development at the L1 larval stage, which we accomplished by placing them in sterile M9 buffer with rocking for 14 h at 25 °C.

Plate loading. In preparation for imaging, groups of 16 assay plates containing worms were placed, top removed, facing down on a glass sheet. We sealed these plates against the glass sheet in a 4×4 grid by means of a rubber mat (**Supplementary Note 1**). The use of this rubber gasket helped to prevent agar from desiccating for the duration of the experiment. When samples were loaded onto scanners, the glass sheets acted as trays to allow for an easy, fast experimental setup.

Plate drying. The plates on which animals were housed during an automated lifespan assay had to be prepared carefully to ensure that the height of the agar matched the modified focal plane of a scanner. The agar for these plates was poured using a peristaltic pump (Wheaton Unispense) and then dried carefully to reach a consistent osmolarity and height. Drying was performed by sealing 75 plates inside a plastic bin containing 942 g of desiccated $CaSO_4$ (Drierite), which, in our experience, absorbs roughly 90 g H_2O/kg. After 12 h at room temperature, the sealed bin reached equilibrium, allowing precise, reproducible plate drying. The weight of Drierite used had to be monitored and adjusted over time, as Drierite appears to gradually become less absorptive. The dimensions of the bin did not appear to play a significant role in the drying process. To reach a final plate osmolality equivalent to the stock recipe, we added an extra 5% of H_2O to our initial mix and calibrated the Drierite mass such that 5% of the each plate's weight was removed during drying. Scanner focus seemed fairly robust to variations in final plate volume; our experiments were performed on plates varying in final weight between 13.2 g and 14.2 g. After drying, plates were sealed and stored at 4 °C until needed. These plates can be seeded with *E. coli* any time after drying.

Temperature calibration of scanners. Scanner temperature was measured by mounting a thermocouple (ThermoWorks USB-REF) on the bottom of an empty Petri dish and loading that dish onto the center of each scanner. Glass sheets and rubber mats were used as described above. We minimized temperature variability by moving scanner power sources outside the incubator and by positioning scanners in a staggered vertical orientation to facilitate airflow throughout the incubator (**Supplementary Note 1**). Scanners produce their own heat and are warmer than ambient incubator temperatures. The temperature gradient between the glass and plates prevented condensation from forming on the glass. To increase the robustness of this effect, we added the antifog coating Rain-X to the surface of the glass trays.

Scanning schedule. Scanning schedules reflected a compromise between heat production, image resolution and scanning speed. Images captured at high resolutions allow nematodes to be distinguished with greater clarity, and a high frequency of capture allows their death times to be identified more precisely. However, high image resolution requires a slower scanning speed, yielding distorted images of moving animals, whereas high capture frequencies allow scanners less time to cool between scans. Therefore, we limited our captures to 3,200-d.p.i. images every 15 min. An additional complication arises in that scanners operate much more slowly when imaging wide areas than they do when imaging narrow strips, perhaps owing to a processing limitation of scanner electronics. To balance these factors, we collected images of

one column (consisting of four plates) at a time rather than all columns at once. In this mode, capture was complete in about 8 min, indicating that the scanner bar moved at an average rate of 400 µm/s. We imaged each column twice in succession, with the first column scanned at time t and $t + 15$ min; the second at $t + 30$ min and $t + 45$ min; the third at $t + 60$ min and $t + 75$ min; and the fourth at $t + 90$ min and $t + 105$ min. The first column was then scanned again at $t + 120$ min, and so on. Hence, every column of four plates was imaged twice in a 2-h cycle, with one short (15-min) and one long (105-min) time interval between successive images of any given plate, a scheme that provided two timescales for movement detection.

Worm identification. Scanners capture images at a lower frequency and lower quality than those attainable with conventional camera-mounted microscopes and thus require more de-noising and image registration (**Supplementary Note 2**). Using only image data, the LM must distinguish worms from other objects present on the plate, such as bacterial clumps and trail shadows. To discriminate between worms and nonworms, we used a support vector machine (SVM)[32] that classifies foreground objects using a set of morphological features (**Fig. 1** and **Supplementary Note 2**). The SVM was trained once with a hand-annotated set of images of worm and nonworm objects. The resultant worm classifier appears to be general, yielding accurate results for young and old animals across strains.

Death determination. In manual lifespan assays, death was declared when an animal failed for the first time to respond to acute stimuli soliciting motion, after which the animal was discarded. The LM does not provide such mechanical stimuli. Instead, it runs a retrospective analysis of posture change to determine the cessation of all spontaneous (as distinct from stimulated) motion, as described in the main text and detailed in **Supplementary Note 5**.

Censoring. An animal may be lost before its death from age is observed; for example, it may get stuck on a plate wall outside the field of view. Such losses cannot be ignored and must be censored to obtain proper survival statistics (**Supplementary Note 8**). Our image analysis maintains a tally of worms at any given scan and uses this to infer worm losses. This process is vitiated when worms aggregate into clusters, inside which our SVM often cannot accurately classify them (**Supplementary Note 2**). After leaving a cluster, worms are again recognized and accounted for. This temporary absence, however, makes it impossible to unambiguously reconstruct the exact timing at which true losses occur. It is nonetheless possible to make reasonable estimates of their timing, as discussed in **Supplementary Note 8**. When two (or more) worms die within a cluster, their death times can be estimated through rapid inspection and annotation of the visual records using the Worm Browser (**Supplementary Video 6** and **Supplementary Note 4**).

Hardware. Please refer to the detailed assembly instructions in **Supplementary Note 3**.

Software. All software can be downloaded at http://www.lifespanmachine.org/.

Imaging servers and image-processing servers. Ten scanners (Epson v700) were housed in each incubator (Thermo Forma 3920). Each group of 20 scanners was controlled by a single Linux server running on consumer PC desktop hardware. Communication was accomplished over USB cables using modified SANE scanner drivers. The servers stored image capture schedules in a MySQL database and executed captures in parallel across multiple scanners. Captured images were buffered to a local disk drive and asynchronously copied to a network storage server. A system that scanned every 15 min over the course of a typical 28-d lifespan experiment generated about 100 GB of compressed image data per scanner (16 plates). Processing intermediates required an additional 100 GB, after which all imagery could be deleted. A central Linux command-and-control server hosted a web interface through which experimental metadata was specified, including scanning schedules and image-processing tasks.

Data inspection and validation software. A cross-platform graphical user interface (GUI) client was developed (the Worm Browser) to facilitate the visual validation and curation of image data banks. Images of each animal can be viewed in aggregate and sorted by their lifespan with this GUI, and time-lapse videos of individual worm deaths can be annotated. The Worm Browser integrates both automated image-analysis results and manual annotations to produce a variety of statistical outputs. Outputs are formatted as comma-separated value (CSV) files for processing by separate statistical packages, including R, JMP and SAS.

Automated survival assay setup times. The time required for one person to complete a 6,000 worm lifespan experiment (as in **Fig. 2**) was as follows. Plate pouring, 3 h; plate drying, 2 h; worm synchronization and transfer to plates with FUDR, 7 h; transfer to assay plates, 4 h; loading plates into scanners and scheduling scans, 1 h; performing 25 °C assay: 0 h (user time)/28 d (chronological time); image analysis and validation, 2.5 h (user)/8 d (computer time on one Quad-Core i7).

Manual lifespan assays. Animals were synchronized and grown at 25 °C as described above and were inspected daily for response to prodding under a dissecting microscope, according to standard practice[6,7]. Dead animals were removed upon identification.

RNA interference. We performed RNAi by feeding as described[24] on plates containing 100 µM ampicillin and 400 µM isopropyl β-D-1-thiogalactopyranoside (IPTG). RNAi bacteria contained either an empty vector (pAD12) or one targeting *daf-2* (pAD48)[24].

UV treatment. For assays performed on UV-treated NEC937 (*E. coli* OP50 $\Delta uvrA::Kan^R$) bacteria[14], killing was accomplished by irradiating freshly seeded plates with 1 J/m^2 of 254-nm light in a UV Stratalinker (Stratagene). Plate sterility was further ensured through addition of 100 µM ampicillin.

Automated stress survival assays. Prior to exposure to 35 °C or *t*-BuOOH, animals were synchronized and grown at 25 °C as described above. Automated survival assays were performed at 35 °C on animals on their second day of adulthood. For *t*-BuOOH survival assays, plates were prepared by adding *t*-BuOOH (Sigma) to a final concentration of 3 mM or 6 mM into molten agar 12 h

before the start of the assay. *E. coli* OP50 was concentrated 5×, resuspended in M9 buffer and used to seed plates. Automated *t*-BuOOH survival assays were performed at 25 °C on animals transferred onto assay plates with *t*-BuOOH on their second day of adulthood. In both 35 °C and *t*-BuOOH survival assays, the assay plates did not contain nystatin or FUDR. In the experiment involving multiple *Caenorhabditis* species, animals were grown on live OP50 bacteria at 20 °C and transferred to 35 °C on the second day of adulthood.

To enable automated analysis of deaths during exposure to high temperature and *t*-BuOOH, we adjusted two image-processing parameters relative to those for unstressed lifespan experiments. First, we reduce the minimum duration of time that animals must cease crawling before being marked as 'stationary'. Second, we reduce the minimum duration of time that animals must be completely motionless before being marked as 'dead'. The movement score threshold used as the criterion for absence of motion remained identical for stress resistance and lifespan assays.

Statistical methods. Log-rank and Wilcoxon tests for homogeneity between two or more survival curves were performed using JMP (SAS)[33] and R[34]. Categorical regression using the Buckley-James estimator[35] was performed in R using the surv and rms packages. Estimates of the piecewise-constant hazard rate were made in R using the muhaz package. Weibull and Gompertz parameters were estimated by parametric regression in R using the flexsurv package.

31. Stiernagle, T. Maintenance of *C. elegans*. in *WormBook* http://dx.doi.org/10.1895/wormbook.1.101.1 (2006).
32. Dong, J.X., Krzyzak, A. & Suen, C.Y. Fast SVM training algorithm with decomposition on very large data sets. *IEEE Trans. Pattern Anal. Mach. Intell.* **27**, 603–618 (2005).
33. Sall, J., Lehman, A., Stephens, M. & Creighton, L. *JMP Start Statistics: A Guide to Statistics and Data Analysis using JMP* 5th edn. (SAS Institute, Cary, North Carolina, 2012).
34. R Development Core Team. *R: A Language and Environment for Statistical Computing* (R Foundation for Statistical Computing, Vienna, 2006).
35. Buckley, J. & James, I. Linear regression with censored data. *Biometrika* **66**, 429–436 (1979).